Available online at www.sciencedirect.com
ScienceDirect
Trans. Nonferrous Met. Soc. China 28(2018) 2053−2061
Transactions of Nonferrous Metals Society of China
www.tnmsc.cn

Preparation of porous Ta−10%Nb alloy scaffold and its in vitro biocompatibility evaluation using MC3T3-E1 cells

Jing-lei MIAO[1,2], Jue LIU[1], Hui-feng WANG[1], Hai-lin YANG[1], Jian-ming RUAN[1]

1. State Key Laboratory of Powder Metallurgy, Central South University, Changsha 410083, China;
2. Department of Orthopedics, The Third Xiangya Hospital of Central South University, Changsha 410013, China

Received 26 October 2016; accepted 8 June 2017

Abstract: A highly porous Ta−10%Nb alloy was successfully prepared for tissue engineering via the methods of the sponge impregnation and sintering techniques. The porous Ta−10%Nb alloy offers the capability of processing a pore size of 300−600 μm, a porosity of (68.0±0.41)%, and open porosity of (93.5±2.6)%. The alloy also shows desirable mechanical properties similar to those of cancellous bone with the elastic modulus and the comprehensive strength of (2.54±0.5) GPa and (83.43±2.5) MPa, respectively. The morphology of the pores in the porous Ta−Nb alloy shows a good interconnected three-dimension (3D) network open cell structure. It is also found that the rat MC3T3-E1 cell can well adhere, grow and proliferate on the porous Ta−Nb alloy. The interaction of the porous alloy on cells is attributed to its desirable pore structure, porosity and the great surface area. The advanced mechanical and biocompatible properties of the porous alloy indicate that this material has promising potential applications in tissue engineering.
Key words: porous Ta−Nb alloy; low elastic modulus; pore structure; in vitro evaluation

1 Introduction

Bone defects, caused by trauma, tumor resection and infection, are of great importance in clinical issues. Generally, the main medical treatments are emphasizing on autograft and allograft transplantations [1,2]. However, the limited bone sources and immune rejection or infection impede the wide clinical application in the reparative treatment. In the past decades, metallic biomedical materials are gaining increasingly interest in the treatment of bone defects [3]. However, the following main issues are persisting in the clinical application of these metallic materials. Firstly, the modulus of the bulk bio-metallic materials is more than 40 GPa, considerably higher than that of human bone, according to the recent reports [4−7]. The high elastic moduli of these materials could always result in preventing the applied stress from transferring along the bones, generating a so-called "stress shielding" effect. Secondly, the toxicity of the metallic ions such as V, Co, Al, and Ni released from metallic materials can generate detrimental biological effects on the complex fluid environment in a human body [8−10]. To avoid using toxic elements, non-toxic elements including Ti, Nb, Ta and Zr, capable of providing good biocompatibility, are becoming a promising trend for the next generation biomedical metallic materials [11−13]. Finally, the bonding strength of the interfaces between metallic biomedical materials and the human muscle or tissue is very important for the longevity of the implants.

To solve the problems, porous materials are becoming feasible for the clinical application of structural bone graft and bone regeneration in recent years [14,15]. Because the size and distribution of the pores in porous materials can be controlled, therefore, the structure modulus can be adjusted to meet the specific requirements according to its corresponding implant bone. Moreover, the porous structure can provide a good biological fixation to the surrounding tissue through inducing bone tissue growing into the porous cell [16]. As alternatives of V, Co, Al, and Ni, the elementals of Ta and Nb can be capable of providing the advantages of outstanding characteristics such as high

Foundation item: Projects (51404302, 51274247) supported by the National Natural Science Foundation of China; Project supported by "125 Talent Project" of the Third Xiangya Hospital of Central South University, China
Corresponding author: Hai-lin YANG, E-mail: y-hailin@csu.edu.cn; Jian-ming RUAN, Tel: +86-731-88876644, E-mail: jian-ming@csu.edu.cn
DOI: 10.1016/S1003-6326(18)64849-6

immunity to corrosion, complete inertness to body environment, enhanced biocompatibility, low modulus and high capacity to join with bone and other tissues, which are gaining much attention as new biomaterials.

Ta and Nb in the same periodic element, having similar properties including good biocompatibility and outstanding corrosion resistant, are new developing biomaterials. However, due to having high melt point (3107 °C) and high density (16.67 g/cm^3), the preparation of Ta-based biomaterials has its intrinsic difficulty. Recently, it was reported that a porous Ta with a porosity of between 65% and 73% was prepared by depositing pure Ta onto a vitreous carbon scaffold [17,18]. Interestingly, it was found that the fatigue endurance limit of the porous Ta at 10^8 cycles was only 13.2 MPa and the elastic modulus was 1.15 GPa. However, the cost in preparation and the residual carbon in the prepared porous Ta should be fully assessed [18]. It should be noted that a novel method of preparing a highly porous Ta was introduced in our lab as well [19]. The prepared porous Ta has the pore size of 300−600 μm, a porosity of 66.7%, an open porosity of 98 %, a compressive elastic modulus of 2.21 GPa and a comprehensive strength of 61.5 MPa, similar to those of cancellous bone. However, the high sintering temperature and the slightly low strength should be further in consideration.

In the present work, we introduce a porous Ta−10%Nb alloy fabricated by a method of integrating the sponge impregnation and sintering technique. We aim to clarify that the effect of Nb on the mechanical property behavior of the porous Ta−10%Nb alloy, so that the porous alloy could have the suitable strength to meet the requirements of human bone. As a comparison, the biological behaviour of Ta−Nb porous alloy, together with porous Ta, was fully assessed by using MC3T3-E1 cells.

2 Experimental

2.1 Fabrication of porous Ta−10%Nb alloy

The start material, tantalum powder used in the experimental with 99.5% purity and average particle size of 10.40 μm was commercially available from Dong Fang Tantalum Co., Ltd., China. NbH powder was of 99.5% purity and the average particle size was 20.57 μm. The porous sponge scaffold, a type of commercial polyurethane purchased from Dongguan Zhanyu Industry & Trade Co., Ltd., China, had interconnected macroporosity, with an open porosity of 50−80 pores per inch (PPI), corresponding to their pore diameters of 500−800 μm. The density of the sponge foam scaffolds was in the range of 0.05−0.07 g/cm^3.

The Ta and NbH powders (10:1, w/w) were blended together in a high energy ball mill at a velocity of 200 r/min for 1 h with the protection of Ar atmosphere. 5% polyvinyl alcohol (PVA) was then added into the blended Ta−10%Nb powder and stirred homogenously to control the viscosity. Subsequently, the pretreated sponge was impregnated in the blended Ta−10%Nb powder slurry. The impregnation process was carried out until the calculated slurry was absorbed completely. After being uniformly impregnated, the specimens were dried in vacuum at 100 °C for 24 h to obtain a firm green body. Finally, the multi-step sinter process was carried out as follows: 1) the temperature was increased up to 300 °C at a rate of 5 °C/min and held for 2 h to make sure that the sponge scaffolds and the PVA were burned out as completely as possible; and 2) the ultimate sintering was carried out at 1850 °C for 2 h in high vacuum (below 9.0×10^{-3} Pa) with the heating/cooling rate of 10 °C/min.

2.2 Material characterization

The apparent porosity and the open porosity of the sintered porous Ta−10%Nb alloy were measured by the Archimedes method, which was described in detail elsewhere [19,20]. Compression tests for mechanical property evaluation were performed by using a universal testing machine (CTM4000) according to GBT8489−2006. Elastic modulus and compressive strength were determined from the stress−strain plots derived from the load−displacement data recorded during the compression testing. The reported data were obtained by averaging the results of 5 samples. All the tests were performed at ambient temperature (~25 °C). A Jeol−6360LV scanning electron microscopy (SEM) was utilized to analyze the microstructure at the cross sections.

2.3 In vitro experiments

2.3.1 Seeding of MC3T3-E1 on porous Ta−10%Nb alloy

Rat osteoblasts MC3T3-E1 cells, purchased from the Center of Cell Resource, Chinese Academy of Science Shanghai Institute for Biological Science, were cultured on 24-well cell culture plates (Greiner) in RPMI 1640 (Thermo) supplemented with 10% (v/v) fetal bovine serum (Thermo), 1% antibiotics and 0.85 mmol/L ascorbic acid-2 phosphate. Herein, to compare in vitro of porous Ta−10%Nb alloy, porous Ta [19] and bulk Ta−10%Nb alloy were also employed in the experimental. Before cell culture, the porous Ta−10%Nb alloy, the porous pure Ta and the bulk Ta−10%Nb alloy were cut by wire-electrode cutting machine into the thickness of 1.5 mm and gently polished with 2000# SiC abrasive grinding paper. All samples were washed repeatedly 3 times using acetone and double distilled water ultrasonically, and then sterilized in a high-pressure autoclave at 120 °C for 30 min for sterilization. Sterilized specimens were incubated with cell seeding

density of 1×10^5 in a humidified incubator containing 5% CO_2 at 37 °C for 5 h. Finally, the scaffolds with seeded cells were transferred to a fresh 96-well plate for further culture.

2.3.2 Adhesion and proliferation of MC3T3-E1 on porous Ta−10%Nb alloy

The adhesion and proliferation were assessed by acridine orange fluorescence staining at the cultured time of 24, 48 and 72 h. Before incubation, the porous Ta, the porous Ta−10%Nb alloy and the bulk Ta−10%Nb alloy were transferred into the 24-well cell plate and were post-fixed. Then, a cell suspension of 1×10^5/mL was seeded on the porous Ta−10%Nb alloy, the porous Ta and the bulk Ta−10%Nb alloy, and wells without any metal discs served as the control (600 μL per well). After incubation, the cells were performed for each sample with 95% ethanol (500 μL/well) for 10 min, and then 300 μL of acridine orange was added into each well. Subsequently, the samples were washed with PBS again, followed by color separation with sodium chloride of 0.1 mmol/L. Total adhered cells were observed and counted by Image-ProPlus6 (IPP6) under fluorescence microscope. Statistical analysis was performed using t-test, and was considered significantly at $P\leq0.05$. Typically, after 72 h cultures, the cell-material complex was isolated, fixed with 3% glutaraldehyde for 30 min, dehydrated with ethanol and dried in vacuum. The dried samples were then gold-coated and observed by SEM.

2.3.3 MTT assay

Prior to MTT test, the porous Ta−10%Nb alloy, the porous Ta and the bulk Ta−10%Nb alloy were cleaned, dried and sterilized by an ultraviolet radiation for at least 2 h. 3 cm^2/mL of serum-free medium was added to each sample and then cultured in a humidified atmosphere with 5% CO_2 at 37 °C for 72 h to obtain the extracts of the materials. For comparison, DMEM media were used as the negative control groups and DMEM media with 10% DMSO were used as the positive control groups. Cells were incubated in 96-well plates at the density of 1×10^5/mL culture medium in each well for 24 h to make sure that the attachment could happen. Then, the medium was replaced by 100 μL of extraction medium. After 0, 24, 48 and 72 h of incubation, 10 μL MTT solution was added to each well and was incubated for 4 h. Then, 100 μL of formazan solubilization solution (10% sodium dodecyl sulfate in 0.01 mol/L HCl) was added to each well. The optical density (OD) of the solution in each well was measured at a wavelength of 570 nm using a microplate reader. The relative growth rate (RGR) was calculated according to the following equation:

$$RGR=OD_{samples}/OD_{negative\ \ control}\times100\% \quad (1)$$

The criteria for cell toxicity classification were defined as: RGR≥100%, level 0; RGR 75%−99%, level I; RGR 50%−74%, level II; RGR 25%−49%, level III; RGR 1%−24%, level IV; RGR 0, level V.

3 Results

3.1 Characterization of porous Ta−10%Nb alloy

Figure 1 shows the microstructure of the porous Ta−10%Nb alloy and the morphology of the pores. It can be seen from Fig. 1(a) that the pore size is around 400 μm and the pores in the porous Ta−Nb alloy have a 3D interconnected open circular or oval cell structure. More detailed observation of the pores is presented in Fig. 1(b). The pore cells are interconnected and the walls of the pore are rough. It is worth pointing out that the skins of pores are continuously connected because of the formation and growth of sintering neck during the sintering process. Overall, the morphologies of dics and rod sample, as indicated in Fig. 1(c), show a good

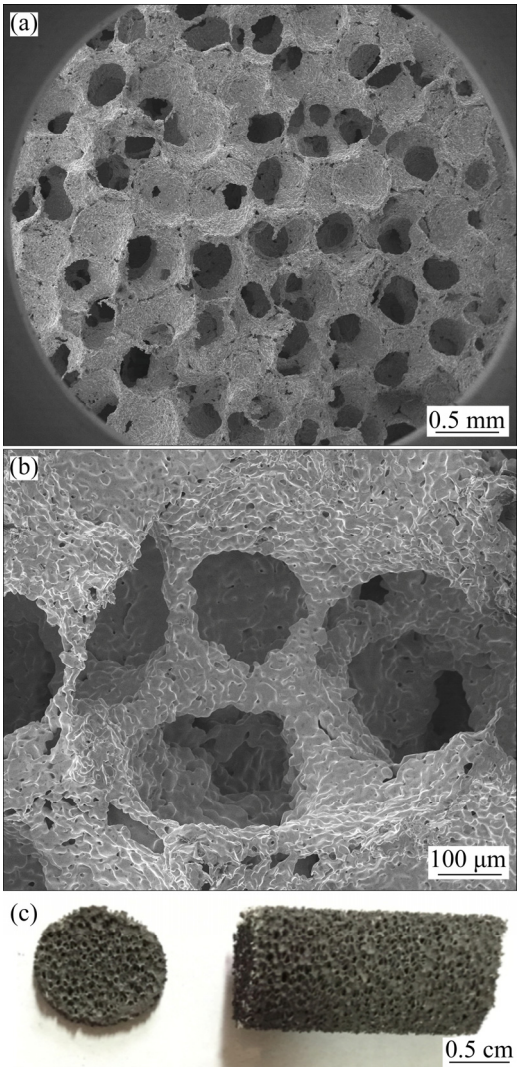

Fig. 1 SEM images showing morphology of porous Ta−10%Nb alloy (a), detailed porous wall of specific pore (b) and representative photos showing cross section and rod bar of sintered porous Ta−10%Nb alloy (c)

stable porous shape in 3-dimension. The XRD pattern of the sintered porous Ta−Nb alloy is shown in Fig. 2. The characteristic peaks clearly showed that it was no visible impurity. This indicated that the diffusion of the sintering process occurred and no obvious impurities (such as C, N, and O) were introduced. The high sintering temperature (1850 °C for 1 h), multi-step sintering process and the vacuum as high as 9×10^{-3} Pa ensured the alloying of Ta−Nb powder and considerably low impurities. The porosity and open porosity of the sintered porous Ta−10%Nb alloy, which were measured by using the Archimedes method, are (68.0±0.41)% and (93.5±2.6)%, respectively.

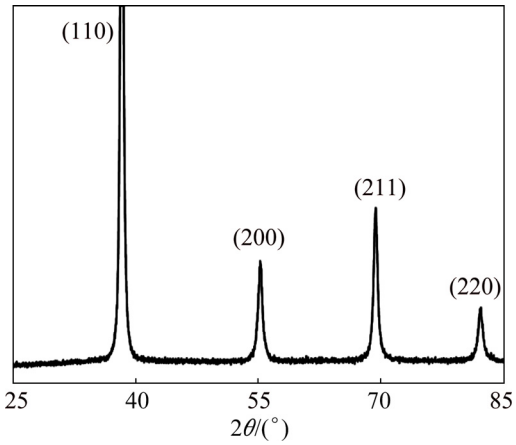

Fig. 2 XRD pattern of sintered porous Ta−10%Nb alloy

Typical stress−strain curve of the porous Ta−Nb alloy during compressive testing is shown in Fig. 3. Obviously, it could be divided into three steps [20]: 1) a linear elasticity region, which could be recoverable because of the elastic deformation, was observed initially, and the elastic modulus was calculated according to the slope of a linear region; the yield point was considered as the compressive strength; 2) a non-linear elasticity region, where a horizontal plateau occurred could be clearly seen. In this stage, the strain cannot be recoverable due to the plastic deformation. The long stress plateau is exploited in foams for crash protection and energy absorbing systems; 3) a collapse and destroy region, in which the porous structure cell of Ta−10%Nb alloy started to be destroyed. Plastic collapse in open-cell foam occurred when the moment exerted on the cell walls exceeded the fully plastic moment creating plastic hinges. According to the stress−strain curve of the 8 samples, the compressive strength and the modulus were (83.43±2.5) MPa and (2.54±0.5) GPa, respectively.

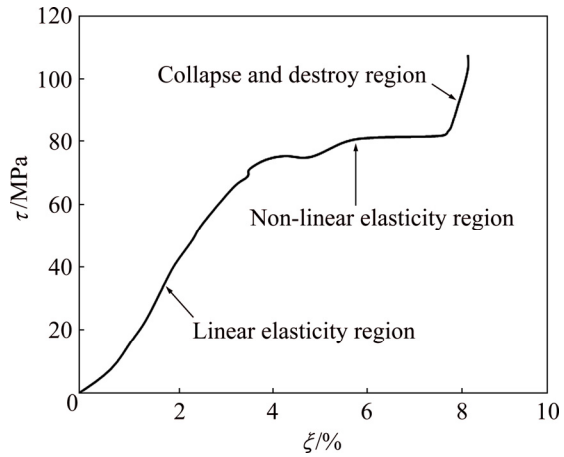

Fig. 3 Typical stress−strain (τ–ξ) curve showing change of compressive process for Ta−10%Nb porous alloy

3.2 Cell culture and proliferation results of MC3T3-E1 on porous Ta−10%Nb alloy

Qualitatively, florescent optical micrographs of the adhesion and proliferation of MC3T3-E1 on porous Ta−10%Nb alloy are presented in Fig. 4. For better comparison, the porous Ta and the bulk Ta−10%Nb alloy were selected to assess their biocompatibility together with the porous Ta−10%Nb alloy. As seen, with increasing inoculation time, the adhesion and proliferation of MC3T3-E1 on three materials showed a significant increase. Moreover, compared with the bulk Ta−10%Nb alloy, the porous Ta−10%Nb alloy and the porous Ta showed evidently much more MC3T3-E1 on their surfaces. This indicated that the introduced porous structure can effectively improve the ability of the adhesion and proliferation of MC3T3-E1. It is worth pointing out that the number of cells on the porous Ta−10%Nb alloy is similar to that on the porous Ta. Furthermore, quantitatively, the total number of MC3T3-E1 of the adhesion and proliferation on the three materials counted by fluorescence microscope using IPP6 software is shown in Fig. 5. As expected, the adhesion and proliferation of MC3T3-E1 on the porous Ta−10%Nb alloy and the porous Ta showed much more rapidly than that of the bulk Ta−10%Nb alloy with increasing inoculation time from 24 to 72 h (P<0.05). And, consistently with florescent optical micrographs of the porous Ta−10%Nb alloy, the total number of MC3T3-E1 of the adhesion and proliferation on the porous Ta−10%Nb alloy and the porous Ta showed a similar trend and was within the statistical margin of error. This indicated that Nb in the porous material showed an invisible influence on the adhesion and proliferation of MC3T3-E1.

Typically, the morphology of MC3T3-E1 on the porous Ta−10%Nb alloy surface after 72 h cultivation is shown in Fig. 6. It can be seen that MC3T3-E1 has a flatter or irregular morphology with the size of 5−20 μm, which partially covered on the surface of the porous Ta−10%Nb alloy scaffold or extended inward the pores. The cells were clustered and abounded with pseudopodium, showing better adhesion and activity.

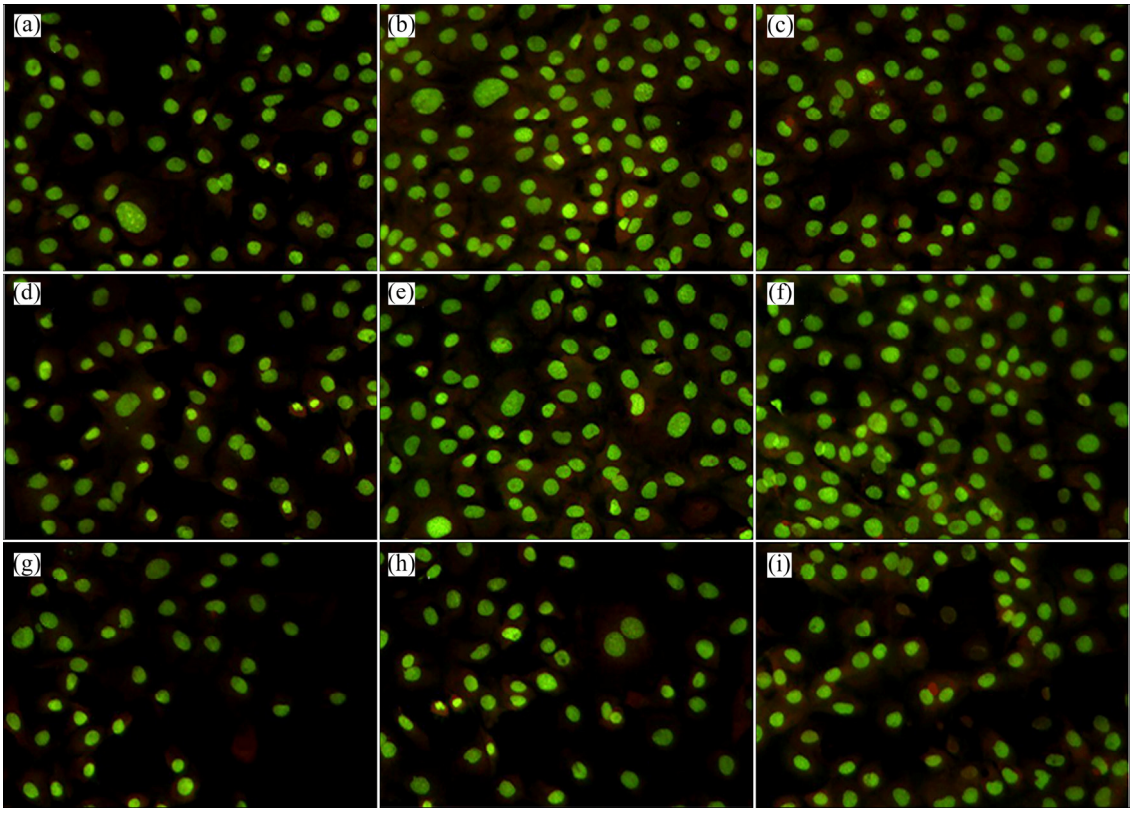

Fig. 4 Florescent optical micrographs of rat MC3T3-E1 on surface of porous Ta−10%Nb alloy (a−c), porous Ta (d−f) and bulk Ta−10%Nb alloy (g−i) cultured for different time: (a, d, g) 24 h; (b, e, h) 48 h; (c, f, i) 72 h

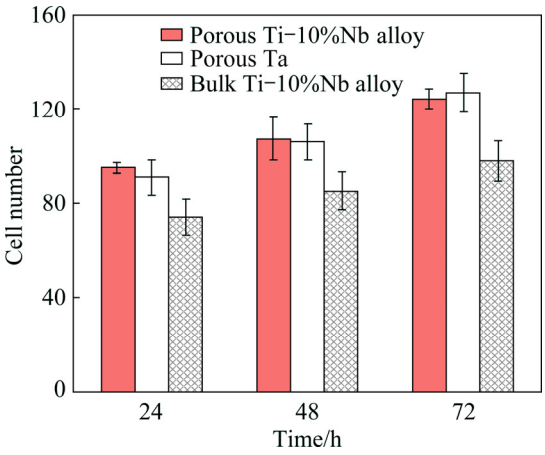

Fig. 5 Cell number of rat MC3T3-E1 calculated by IPP6 software adhering on three kinds of materials for different cultured time

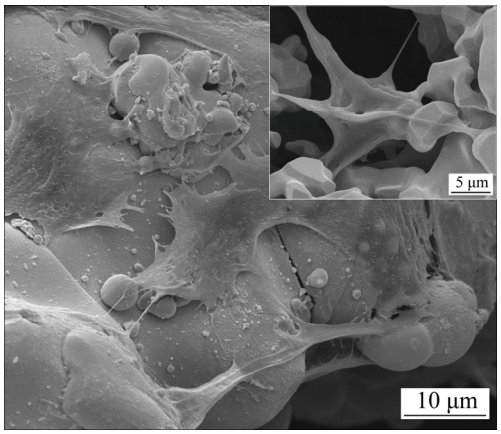

Fig. 6 SEM image of rat MC3T3-E1 on porous Ta−10%Nb alloy surface after being cultured for 72 h at ambient environment (25 °C)

3.3 Cytotoxicity results of MC3T3-E1 on porous Ta−10%Nb alloy

The MTT assay was utilized to quantitatively determine the proliferation of the viable MC3T3-E1 on the porous Ta−10%Nb alloy, the porous Ta and the bulk Ta−10%Nb alloy, as shown in Fig. 7. The viable cell densities of MC3T3-E1 for the porous Ta−10%Nb alloy, the porous Ta, the bulk Ta−10%Nb alloy, negative group and positive group after different cultivation time of 0, 24, 48 and 72 h were compared. As seen, the optical density of the porous Ta−10%Nb alloy and the porous Ta is significantly higher than that of the bulk Ta−10%Nb alloy and is just slightly lower than that of the negative group. Furthermore, the results of toxicity of the three materials by the MTT assay revealed that the RGR values of cells were in the range of 95%−101%, indicating that porous materials were insignificant cytotoxicity (Level I).

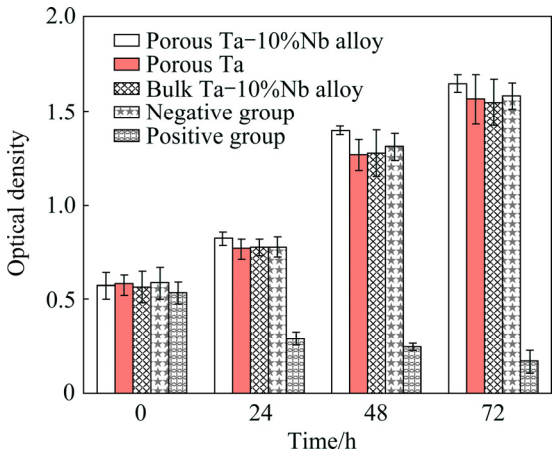

Fig. 7 MTT assay of porous Ta−10%Nb alloy, porous Ta and bulk Ta−10%Nb alloy cultured for different time

4 Discussion

4.1 Sintering behaviour and biomechanical properties

Of all the metallic materials, Ta has the excellent biocompatibility and corrosion resistant and is widely used in biomedical application [21,22]. Whereas, the melting point of Ta (as high as 3017 °C) as well as the high density (16.65 g/cm^3) impedes its further application as a biomedical material for its considerably high cost in preparation. As the same periodic element, Nb has a lower melt point of 2468 °C than Ta, and the density is 8.57 g/cm^3. Therefore, in the present experimental, we aim to use Nb to partially replace Ta and utilize the diffusion of lower melt point Nb during the sintering process to promote the growth at the sintering necks, and finally enhance the mechanical properties. Figure 8(a) presents the detailed microstructure showing the grain boundaries of the porous Ta−10%Nb alloy. It can be observed that the grains were very clear and the sizes were in the range of 5−10 μm, which were due to the growth of sintering necks and the merge of grains. During the sintering process, on one hand, the lower melt point Nb started to diffuse and part of Nb solutionized into tantalum. The solution of Nb in Ta made the melt point reduce, which intensified the solid phase sintering process. The improved bonding between the grain boundaries which formed due to the growth of sintering neck, in turn, promoted the mechanical properties. In our previous work [19], the compressive strength and elastic modulus of the porous Ta, which was sintered at 1950 °C, were (61.5±4.5) MPa and (2.21±0.16) GPa, respectively. In the present work, the compressive strength and the elastic modulus were much improved up to (83.43±2.5) MPa and (2.54±0.5) GPa, respectively. The improvement in the mechanical properties is believed to be attributed to the solution strengthening by the alloying of Nb in the Ta−Nb alloy and the low sintering temperature. Furthermore, Table 1 lists the mechanical

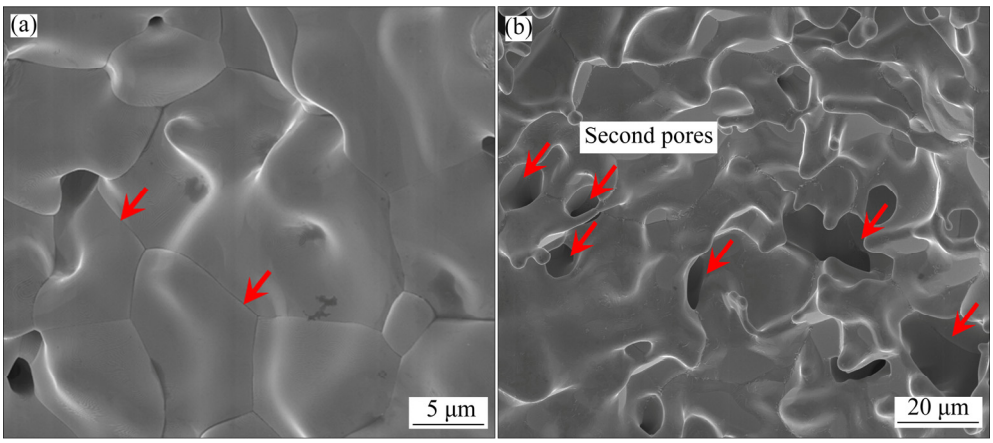

Fig. 8 SEM images showing grain boundaries formed after sintering necks growth (a) and second pores with size in range of 5−20 μm on pore wall (b) for porous Ta−10%Nb alloy

Table 1 Comparison of physical mechanical properties of porous Ta and porous Ta−10%Nb alloy with cancellous bone and cortical bone

Material	Porosity/%	Density/(g·cm^{-3})	Compressive strength/MPa	Elastic modulus/GPa
Porous Ta [19]	66.7±0.23	6.18±0.25	61.5±4.5	2.21±0.16
Porous Ta−10%Nb alloy	68.0±0.41	4.87±0.16	83.43 ± 2.5	2.54±0.5
Cancellous bone [15]	30−90	−	10−50	0.01−3.0
Cortical bone [15]	5−30	−	130−150	4.4−28.8

properties of the porous Ta and the porous Ta−10%Nb alloy together with the the parameters of cancellous bone and cortical bone. The porous Ta and the porous Ta−10%Nb alloy have a similar porosity of around 70%, which is in the range of cancellous bone. Due to the addition of 10% Nb, the density dropped down from (6.18±0.25) to (4.87±0.16) g/cm^3, which is 20% lower than that of the porous Ta in the application of clinic. The improved strength and suitable elastic modulus could also offer high strength and stability to meet the requirement of human bone.

Additionally, the second pores in the wall of the pores, which are formed in the sintering process, are the unique characteristic of the porous Ta−Nb alloy. As shown in Fig. 8(b), there were many second pores distributed on the wall of the pores and the sizes of the pores are in the range of 5−20 μm. The formation of these second pores could be attributed to the shrinkage of the sintered powder particles. During the process of impregnation, the sponge scaffold was immersed into the blended suspension liquid. And then, the skin of the sponge delivered the suspension liquid to different inter-connected surfaces of the pores because of the drive of capillary force. Subsequently, in the following dry process at high vacuum, the water in the PVA was evaporated; the powder particles were bonded together and stuck on the skin of pores. In the final sintering process, the pore sizes came to shrink through gradual elimination of the sponge scaffold and mechanical bonding of the solid particles. Meanwhile, the particles began to immerge and grow to form the grains and the shrinkage thus occurred. The bonding of the particles, thereby, left many second pores behind the wall of the pores, as shown in Fig. 8(b).

4.2 Biocompatibility behaviour

First of all, porous structure cells of the porous materials are expected to offer a larger surface interaction area with the cells by offering mechanical anchoring sites, resulting in facilitating the growth of the cells [4]. The specific size of the pores, which is optimum for in-growth of human bone tissues, should be within a specific range. A porous structure cell of the metallic materials could offer spaces for bone cells, vascular and bone tissue ingrowth to form mechanical interlocking which, in turn, encourages osteointegration and prevents implantation failure [23,24]. Increasingly, a number of investigations have identified that the pore size of 100−600 μm can more easily enhance the bone tissue ingrowth and eventually good implant fixation [25−27]. Our previous results [19,23,28] also indicated that the size of 300−600 μm of the porous Ta, the porous Ti−Ni alloy and the porous Ti−25%Nb alloy can evidently promote the cells to ingrowth. Another important aspect is that the connectivity of porous material is extremely helpful. Because the connected pores are of great importance for adhesion, proliferation and differentiation when the cells are attached to the material surface. The connected pores could offer the connected channels for nutrient delivery and waste removal. Early and stable osteointegration at the interface between metallic bone implant materials and a bony site is one of the most important indicators of clinical success (new bone formation) [29]. As mentioned before, the second pores on the walls of the Ta−10%Nb alloy offer anchoring place for the cells to attach. The early and stable osteointegration is of great importance for the forthcoming attachment, differentiation and proliferation. One of the most important surface properties of the implants is the surface energy, which presents the surface wettability. The wettability of an implant material influences the degree of the contact and interaction between the implant and the biological environment [30,31]. Influences of the surface energy on protein adsorption, osteoblast adhesion, spreading and proliferation have been extensively studied [32]. As well as our previous investigations, the second pores in the range of 5−20 μm can offer a considerably good fixation of earlier cell attachment due to the large surface area and the roughness of the pore surfaces, which is in accordance with the other findings [33−35].

The chemical components of the implant alloy play a significant role in determining the interaction between the implant materials and their surrounding tissues. As mentioned before, Ta and Nb have excellent biocompatibility. In the present work, the 3D interconnected open cell structure provides the similar and proper growing space and structure microenvironment for the seeded cells, where they are located on the porous structure. During enhancement of the bone tissue ingrowth and eventually good implant fixation, these open structure characteristics play a positive role by promoting capillary phenomena [3]. For a long term, spontaneously formed oxides, whose compositions are Ta_2O_5 and Nb_2O_5, will provide a bio-inert layer on the alloy surfaces in the complex human body fluids [36]. Thereby, the enrichment of Ta_2O_5 and Nb_2O_5 on the surface suppresses the dissolution of Ti and Nb as ions. So, the Ta−10%Nb alloy shows a high cell viability during the MTT assay.

5 Conclusions

1) With a high porosity of (68.0±0.41)% and a 3D interconnected open porosity of (93.5±2.6)%, the Ta−10%Nb alloy was successfully prepared by combination of the sponge impregnation and sintering

techniques. The porous Ta−Nb alloy can be capable of having the pore size of 300−600 μm, the compressive strength of (83.43±2.5) MPa, and the compressive elastic modulus of (2.54±0.5) GPa.

2) The in vitro results revealed that the highly porous Ta−10%Nb alloy have good biocompatibility, which can significantly promote adhesion and proliferation of MC3T3-E1 cells. It is indicated that the porous Ta−10%Nb alloy can induce osteoblasts to penetrate into the pores and interconnected channels, offering good biological fixation. All these data provide proofs further that the porous Ta−10%Nb alloy is one of highly promising candidates of advanced biomaterials in tissue engineering.

Acknowledgments

The author Hai-lin YANG would like to acknowledge the financial support from the independent project of State Key Laboratory of Powder Metallurgy and useful discussion and suggestion with Dr. Shou-xun JI and Yun WANG from Brunel University London.

References

[1] LAURENCIN C T, KHAN Y, EL-AMIN S F. Bone graft substitutes [J]. Expert Review of Medical Devices , 2006, 3(1): 49−57.

[2] MCALLISTER D R, JOYCE M J, MANN B J, VANGSNESS C T J R. Allograft update the current status of tissue regulation, procurement, processing, and sterilization [J]. The American Journal of Sports Medicine, 2007, 35(12): 2148−2158.

[3] AMINI A R, LAURENCIN C T, NUKAVARAPU S P. Bone tissue engineering: Recent advances and challenges [J]. Critical Reviews in Biomediacl Engineering, 2012, 40(5): 363−408.

[4] LIU Y, LI K, WU H, SONG M, WANG W, LI N, TANG H. Systhesis of Ti−Ta alloys with dual structure by incomplete diffusion between elemental powders [J]. Journal of the Mechanical Behavior of Biomedical Materials, 2015, 51: 302−312.

[5] HAO Y L, LI J, SUN S Y, ZHENG C Y, YANG R. Elastic deformation behaviour of Ti−24Nb−4Zr−7.9Sn for biomedical applications[J]. Acta Biomaterialia, 2007, 3(2):277−286.

[6] BONISCH M, CALIN M, HUMBEECK J V, SKROTZKI W, ECKERT J. Factors influencing the elastic moduli, reversible strains and hysteresis loops in martensitic Ti−Nb alloys [J]. Materials Science and Engineering C, 2015, 48(1): 511−520.

[7] CALIN M, HELTH A, MORENO J G, BONISCH M, BRACKMANN V, GIEBELER L, GEMMING T, LEKKA C E, GEBERT A, SCHNETTLER R, ECKERT J. Elastic softening of β-type Ti−Nb alloys by indium (in) additions [J]. Journal of the Mechanical Behavior of Biomedical Materials, 2014, 39: 132−174.

[8] HILDEBRAND H F, VERON C, MARTIN P. Nickel, chromium, cobalt dental alloys and allergic reactions: an overview [J]. Biomaterials, 1989, 10(8): 545−548.

[9] OKAZAKI Y, GOTOH E. Metal ion effects on different types of cell line, metal ion incorporation into L929 and MC3T3-E1 cells, and activation of macrophage-like J774.1 cells [J]. Materials Science and Engineering C, 2013, 33(4): 1993−2001.

[10] PERL D P, BRODY A R. Alzheimer's disease: X-ray spectrometric evidence of aluminium accumulation in neurofibrillary tangle bearing neurons [J]. Science, 1980, 208(4441): 297−299.

[11] XU Yan-fei, XIAO Yi-feng, YI Dan-qing, LIU Hui-qun, WU Liang, WEN Jing. Corrosion behavior of Ti−Nb−Ta−Zr−Fe alloy for biomedical applications in Ringer's solution [J]. Transactions of Nonferrous Metals Society of China, 2015, 25: 2556−2563.

[12] SHARKEEV Y, KOMAROVA E, SEDELNIKOVA M, SUN Ze-ming, ZHU Qi-fang, ZHANG Jing, TOLKACHEVA T, UVARKIN P. Structure and properties of micro-arc calcium phosphate coatings on pure titanium and Ti−40Nb alloy [J]. Transactions of Nonferrous Metals Society of China, 2017, 27: 125−133.

[13] MIYAZAKI T, KIM H, KOKUBO T, OHTSUKI C, KATO H, NAKAMURA T. Mechanism of bonelike apatite formation on bioactive tantalum metal in a simulated body fluid [J]. Biomaterials, 2002, 23: 827−832.

[14] MUTLU I. Synthesis and characterization of Ti−Co alloy foam for biomedical applications [J]. Transactions of Nonferrous Metals Society of China, 2016, 26: 126−137.

[15] GEETHA M, SINGH A K, ASOKAMANI R, GOGIA A K. Ti based biomaterials, the ultimate choice for orthopaedic implants: A review [J]. Progress in Materials Science, 2009, 54: 397−425.

[16] HUANG H H, WU P, SUN Y S, YANG W E, LIN M C, LEE T H. Surface nanoporosity of β-type Ti−25Nb−25Zr alloy for the enhancement of protein adsorption and cell response [J]. Surface and Coatings Technology, 2014, 259(Part B): 206−212.

[17] SEVILLA P, APARICIO C, PLANELL J, GIL F. Comparison of the mechanical properties between tantalum and nickel-titanium foams implant materials for bone ingrowth applications [J]. Journal of Alloys and Compounds, 2007, 439: 67−73.

[18] ZARDIACKAS L D, PARSELL D E, DILLON L D, MITCHELL D W, NUNNERY L A, POGGIE R J. Structure, metallurgy, and mechanical properties of a porous tantalum foam [J]. Journal of Biomedical Materials Research Applied Biomaterials, 2001, 58: 180−187.

[19] YANG Hai-lin, LI Jing, ZHOU Zhong-cheng, RUAN Jian-ming. Structural preparation and biocompatibility evaluation of highly porous tantalum scaffolds [J]. Materials Letters, 2013,100: 152−155.

[20] JIE Yun-feng, ZOU Jian-peng, RUAN Jian-ming. Fabrication of porous niobium-based biological materials via impregnation and their properties [J]. Rare Metal Materials and Engineering, 2010, 39(11): 2015−2017

[21] MARTINO I D, SANTIS V D, SCULCO P K, D'APOLITO R, POULTSIDES L A, GASPARINI G. Long-term clinical and radiographic outcomes of porous tantalum monoblock acetabular component in primary hip arthroplasty: A minimum of 15-year follow-up [J]. Journal of Arthroplasty, 2015, 31(9): 110−114.

[22] WAUTHLE R, STOK J V D, YAVARI S A, HUMBEECK J V, KRUTH J P, ZADPOOR A A, WEINANS H, MULIER M, SCHROOTEN J. Additively manufactured porous tantalum implants [J]. Acta Biomaterialia, 2015, 14: 217−225.

[23] RUAN Jian-ming, YANG Hai-lin, WENG Xiao-jun, MIAO Jing-lei, ZHOU Ke-chao. Preparation and characterization of biomedical highly porous Ti−Nb alloy [J]. Journal of Materials Science: Materials in Medicine, 2016, 27(4): 1−8.

[24] CHEN Q, THOUAS G A. Metallic implant biomaterials [J]. Materials Science and Engineering R, 2015, 87: 1−57.

[25] DAMIEN C J, PARSONS J R. Bone graft and bone graft substitutes: A review of current technology and applications [J]. Journal of Applied Biomaterials, 1991, 2(3): 187−208.

[26] KARAGEORGION V, KAPLAN D. Porosity of 3D biomaterial scaffolds and osteogenesis [J]. Biomaterials, 2005, 26: 5474−5491.

[27] TSURGA E, TAKITA H, ITOH H, WAKISAKA Y, KUBOKI Y. Pore size of porous hydroxyapatite as the cell-substratum controls BMP-induced osteogenesis [J]. Journal of Biochemistry, 1997, 121(2): 317−324.

[28] LI Jing, YANG Hai-lin, WANG Hui-feng, RUAN Jian-ming. Low elastic modulus titanium-nickel scaffolds for bone implants [J].

Materials Science and Engineering C, 2014, 34:110−114.
[29] GOODMAN S B, YAO Z, KEENEY M, YANG F. The future of biologic coatings for orthopaedic implants [J]. Biomaterials, 2013, 34(13): 3174−3183.
[30] SARTORETTO S C, ALVES A T N N, RESENDE R F B, CALASANS-MAIA J, GRANJEIRO J M, CALASANS-MAIA M D. Early osseointegration driven by the surface chemistry and wettability of dental implants [J]. Journal of Applied Oral Science, 2015, 23(3): 279−287.
[31] GITTENS R A, SCHEIDELER L, RUPP F, HYZY S L, GEIS-GERSTORFER J ,SCHWARTZ Z, BOYAN B D. A review on the wettability of dental implant surfaces II: Biological and clinical aspects [J]. Acta Biomaterialia, 2014, 10(7): 2907−2918.
[32] WANG X, LI Y, LIN J, HODGSON P, WEN C. Apatite-inducing ability of titanium oxide layer on titanium surface: The effect of surface energy [J]. Journal of Materials Research, 2008, 23(6): 1682−1688.
[33] WANG X, LI Y, XIONG J, HODGSON P D, WEN C E. Porous TiNbZr alloy scaffolds for biomedical applications [J]. Acta Biomaterialia, 2009, 5: 3616−3624.
[34] NOURI A, HODGSON P D, WEN C. Effect of ball-milling time on the structural characteristics of biomedical porous Ti−Sn−Nb alloy [J]. Materials Science and Engineering C, 2011, 31: 921−928.
[35] POSTIGLIONE L, DI DOMENICO G, RAMAGLIA L, MONTAGNANI S, SALZANO S, DI MEGLIO F, SBORDONE L, VITALE M, ROSSI G. Behavior of SaOS-2 cells cultured on different titanium surfaces [J]. Journal of Dental Research, 2003, 82: 692−696.
[36] MATSUNO H, YOKYAMA A, WATARI F, UO M, AWASAKI T. Biocompatibility and osteogenesis of refractory metal implants, titanium, hafnium, niobium, tantalum and rhenium [J]. Biomaterials, 2001, 22: 1253−1262.

多孔 Ta−10%Nb 支架制备及其体外生物性能评价

苗惊雷[1,2]，刘 珏[1]，王汇丰[1]，杨海林[1]，阮建明[1]

1. 中南大学 粉末冶金国家重点实验室，长沙 410083；
2. 中南大学 湘雅附属三医院 骨科，长沙 410013

摘 要：通过海绵浸渍法和烧结技术制备得到组织工程用的高孔隙 Ta−10%Nb 支架材料，该材料的孔隙尺寸为 300~600 μm，孔隙率达到(68.0±0.41)%，同时开孔率高达(93.5±2.6)%。研究表明，制备得到的 Ta−10%Nb 支架材料具有与人体骨组织相似的弹性模量(2.54±0.5) GPa 和抗压强度(83.43±2.5) MPa。同时，这种材料具有良好的三维空间结构单元，通过在该材料上进行鼠 MC3T3-E1 细胞共培养发现，细胞能很好地粘附生长和增殖。该材料所具备的良好生物力学性能和生物相容性能，使其在生物医学组织工程支架材料应用中具有良好的应用前景。这种多孔金属材料拥有良好的孔隙结构单元、适当的孔隙率以及大的表面积，使得该材料与细胞发生良好的作用。

关键词：多孔 Ta−Nb 合金；低弹性模量；多孔结构；体外评价

(Edited by Xiang-qun LI)